ACS APPLIED MATERIALS & INTERFACES

www.acsami.org

Research Article

Highly Flexible Transparent Micromesh Electrodes via Blade-Coated Polymer Networks for Organic Light-Emitting Diodes

Juan Zhu, Donggeon Han, Xiaodong Wu, Jonathan Ting, Shixuan Du, and Ana C. Arias*

Cite This: *ACS Appl. Mater. Interfaces* 2020, 12, 31687−31695

Read Online

ACCESS | Metrics & More | Article Recommendations | Supporting Information

ABSTRACT: The availability of transparent conductive thin films that exhibit mechanical flexibility and are adapted to low-cost and large-area fabrication is a major obstacle for high-performance flexible thin-film optoelectronics. Here, by combining printing, thin-film deposition, and wet-etching processes, interconnected transparent metal micromesh (TMM) electrodes are reported. Blade-coating is used to generate self-assembled polymer micromesh networks on flexible substrates. The network structures are subsequently converted into conductive metal networks. As-fabricated TMM films display a surface roughness of around 20 nm with thickness down to 50 nm. A transmittance of 86% and a conductance of 80 Ω sq^{-1} are achieved at the described optimal blade-coating suspension concentration. The electrodes show mechanical flexibility with no conductivity degradation with the smallest bending radius of 1 mm or at repeated bending over 3000 cycles at a bending radius of 15 mm. We successfully demonstrate organic light-emitting diodes (OLEDs) using TMM electrodes via the blade-coating technique. The printed OLEDs have a low turn-on voltage of 3.4 V and can achieve a luminance of over 4000 cd/m^2 at 6.5 V. At a luminance of 100 cd/m^2, the OLEDs show a current density of 7.6 mA/cm^2, an external quantum efficiency (EQE) of 3.6%, and a luminous efficacy of 1.4 lm/W.

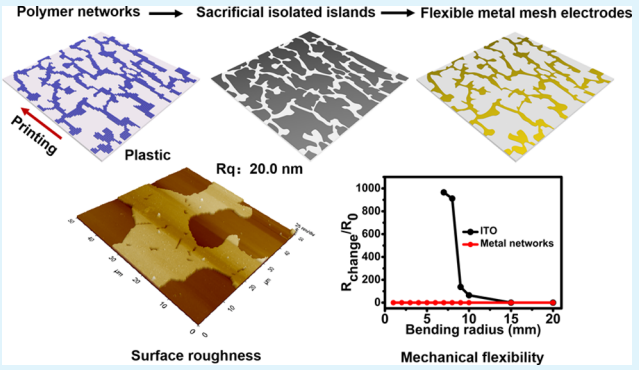

KEYWORDS: *flexible transparent electrodes, micromesh, polymer networks, printing, organic light-emitting diodes*

1. INTRODUCTION

The rapid development of flexible optoelectronics in diverse applications, such as wearable medical devices and touch screens, has prompted scientists to develop flexible transparent conducting electrode materials.[1−9] Thin films of indium tin oxide (ITO) electrodes, the predominant candidates for transparent electrodes in rigid counterparts, offer excellent electronic performances. However, film brittleness, low material abundance, and infrared transmittance have limited the applications of ITO electrodes in flexible electronics and sensors. Alternatives to ITO have been studied intensively and developed including polymers and carbon nanotubes (CNTs).[1,10] Although their flexibility is improved, the low conductivity of these carbon-based materials disables their function in optoelectronic devices that require high conductivity. Graphene has been developed for flexible transparent electrodes. However, the high growth temperature of around 1000 °C limits its direct application on flexible substrates. Metal nanowire-based networks are another alternative. For further usage in optoelectronic devices, wire-to-wire junction resistance must be minimized in the annealing process beyond the tolerance of plastics and a thick planarization layer is needed to decrease film surface roughness.[11−14]

Interconnected metal networks show comparable conductivity and transparency to ITO while providing improved flexibility over ITO. Several novel techniques have emerged to complement the traditional techniques based on expensive photolithography and e-beam lithography. Nanosphere lithography was demonstrated to create metal nanopore transparent networks using a close-packed nanosphere monolayer, which has strict requirements with substrate surface energy and flatness.[15,16] Nanoimprint lithography was used to make semitransparent metal grids, but this method needs soft molds duplicated from photolithography-generated silicon molds.[17] Electron-spun polymer fiber networks,[18,19] grain boundary lithography,[20] and vapor dealloying of ultrathin Au−Cu[21] were applied to get transparent mesh electrodes, where the fabrication process requires a transfer process to flexible substrates or involves high temperatures. Interconnected metal networks can potentially be fabricated by printing techniques,

Received: April 21, 2020
Accepted: June 16, 2020
Published: June 16, 2020

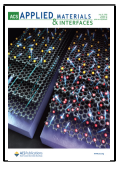

https://dx.doi.org/10.1021/acsami.0c07299
ACS Appl. Mater. Interfaces 2020, 12, 31687−31695

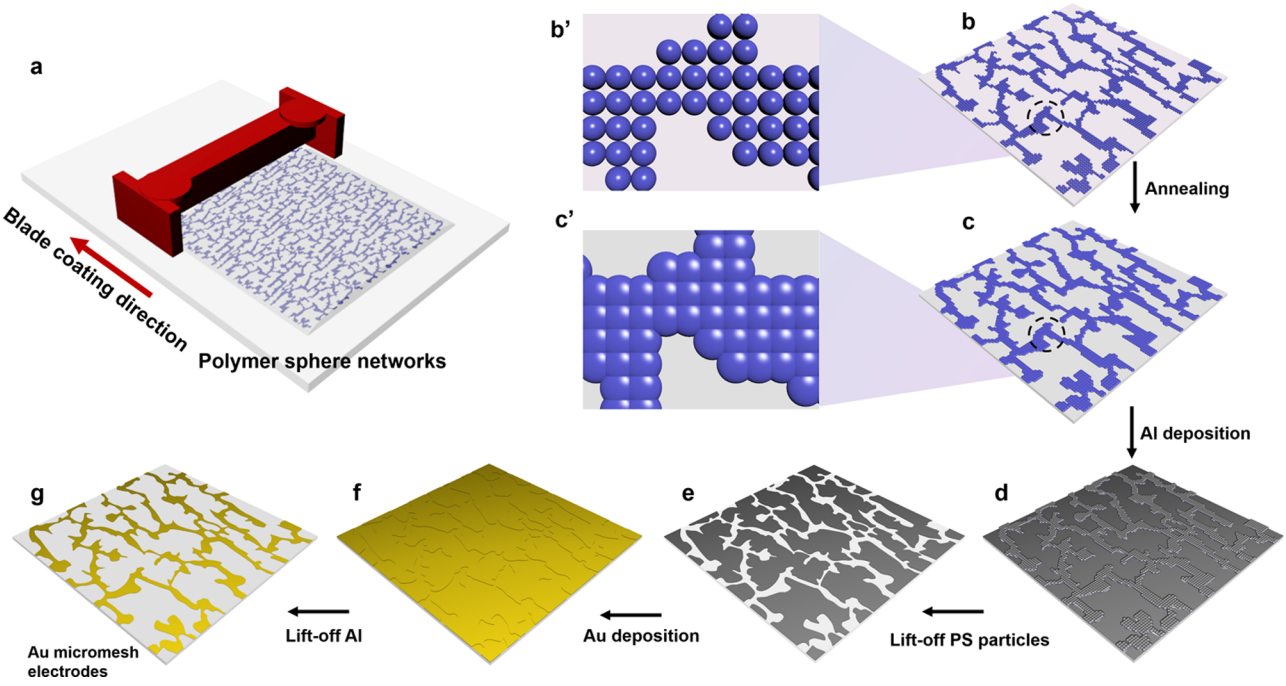

Figure 1. Schematic for the fabrication process of Au micromesh transparent electrodes. Polymer sphere networks were first made on the flexible substrate by blade-coating (a, b, b′) and then annealed to form fully connected networks (c, c′). The polymer networks were coated with Al using thermal evaporation (d) and then lifted off in toluene, leaving Al islands (e). The Al islands were coated with Au using thermal evaporation (f) and then lifted off in dilute HCl solution, forming Au transparent electrodes (g).

which is highly desirable due to their compatibility with large area and high throughput. Reverse-offset printing has been used to realize transparent electrodes.[22] The printed metal films are typically over 100 nm in thickness, which is difficult to use in high-performance optoelectronic devices that require a smooth electrode surface.[23] However, toward the development of large-area flexible electronics, the preparation of thin flexible metal networks by a print-compatible technique remains a critical challenge.

Blade-coating is a very attractive printing technique because it is simple, has high throughput, consumes only a small amount of material, and can realize thickness control of deposited materials by tuning the coating parameters. The ink is deposited in front of the blade and the blade removes excess inks, resulting in uniform thin films on the substrate. Blade-coating has been used to get condensed polymer thin films, working as conductors or semiconductors in thin-film electronic devices.[24,25] In comparison, few studies have focused on developing blade-coating to create network structures.

Among the optoelectronic devices, organic light-emitting diodes (OLEDs) have the most stringent requirements for the transparent electrodes including conductivity, transparency, and surface roughness. Transparent metal networks have been successfully applied in vacuum-deposited and spin-coated OLED devices.[3,17] Compared to conventionally evaporated or spin-coated OLEDs, printed OLEDs reduce material consumption, simplify fabrication procedures, and reduce the cost. Recently, OLEDs were printed on ITO electrodes via blade-coating, and the devices were successfully used as medical optical sensors.[26] Therefore, investigations on the applications of novel flexible transparent electrodes for printing OLEDs are highly needed.

Here, we demonstrate a novel fabrication technique for flexible transparent electrodes by combining printed polymer networks, thin-film evaporation, and wet-etching processes. Blade-coating is used to get spontaneously formed polymer micromesh networks directly on the flexible substrate, and the polymer networks' structures can be duplicated into transparent metal micromesh (TMM) electrodes. This print-compatible technique does not require template usage and transfer processes and can be processed at low temperatures and scaled to large-area fabrication. The TMM electrodes also exhibit remarkable mechanical flexibility under bending stresses. The micromesh electrodes show a thickness below 50 nm. The as-prepared transparent electrodes are further demonstrated in printed OLEDs using blade-coating.

2. RESULTS AND DISCUSSION

2.1. TMM Electrode Fabrication. The fabrication process combines blade-coating, thin-film deposition, and the lift-off process (Figure 1). A polystyrene (PS) sphere suspension in water is first blade-coated on a flexible poly(ethylene terephthalate) (PET) or poly(ethylene naphthalate) (PEN) substrate at 85 °C to form a PS network (Figures 1a,b,b′). Uniform sphere networks formed in the blade-coating process are due to the Rayleigh instability. The temperature of the substrate is increased during the blade-coating process to speed up the evaporation of water. The substrate is then heated at 120 °C higher than the PS glass transition temperature of 100 °C to merge the polymer spheres forming interconnected PS micromesh networks (Figures 1c,c′). It is notable that a viscous polymer tends to form a condensed film instead of porous structures when the polymer is coated by conventional techniques including spin-coating and blade-coating. The combination of blade-coated polymer spheres and annealing in this work provides a method for polymer micronetwork fabrication. A sacrificial aluminum (Al) layer is deposited onto the PS micromesh networks by thermal evaporation (Figure

https://dx.doi.org/10.1021/acsami.0c07299
ACS Appl. Mater. Interfaces 2020, 12, 31687−31695

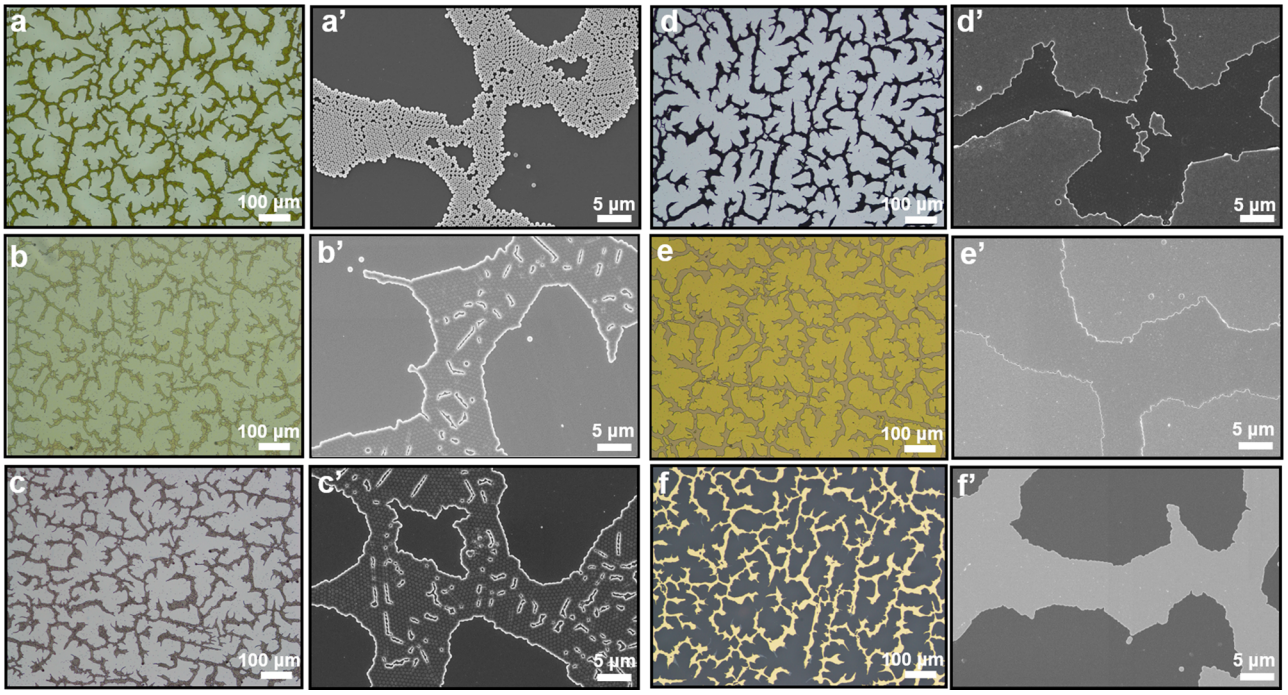

Figure 2. Morphology evolution in each step for the fabrication process of the TMM electrodes. (a-f) Microscope images of microstructures, demonstrating large-area uniformity of the microstructures. (a′-f′) High-magnification SEM images of microstructures, showing further details. (a, a′) PS sphere networks blade-coated on the plastics. (b, b′) Interconnected PS networks after annealing. (c, c′) Sacrificial Al layer deposited on the as-prepared plastics. (d, d′) Al isolated islands after dissolving PS spheres in a dilute HCl solution. (e, e′) Au layer deposited on the plastics. (f, f′) Au network electrodes on the plastics, showing the smoothness of the structure.

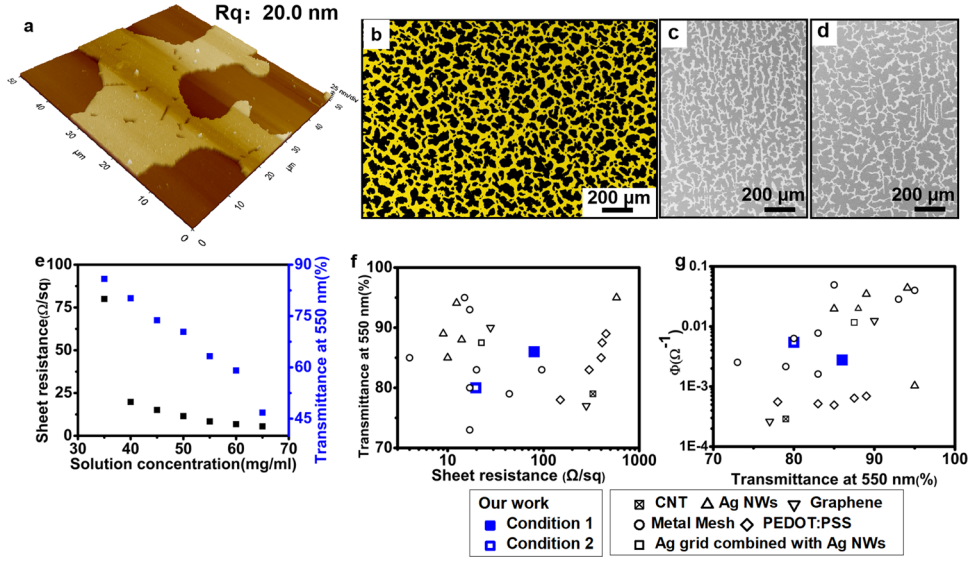

Figure 3. Performance of Au TMM electrodes. (a) Three-dimensional atomic force microscopy (3D AFM) image of the micromesh electrodes on the PET substrate showing a root-mean-square surface roughness of around 20.0 nm. (b) False-color SEM image of the micromesh electrodes prepared with a solution concentration of 65 mg/mL. (c, d) SEM images of the micromesh electrodes prepared with solution concentrations of 50 and 40 mg/mL, respectively. (e) Sheet resistance and optical transmission (at 550 nm) of the TMM electrodes versus solution concentration. (f) Sheet resistance versus optical transmittance for micromesh electrodes fabricated with different solution concentrations: 35 mg/mL (condition 1) and 40 mg/mL (condition 2). (g) FoM (ϕ) of our micromesh electrodes as a function of the optical transmittance (at 550 nm). The performances of carbon nanotubes,[5] graphene,[31,32] PEDOT:PSS,[33] Ag nanowires,[5] Ag grid combined with Ag nanowires,[34] and metal meshes[3,17−21,23,35,36] by other techniques are shown for comparison in panels (f) and (g). Note that the transmittance mentioned here does not include the transmittance of the substrate.

1d). Al is chosen for the sacrificial layer due to its lift-off feasibility in a dilute hydrochloric acid (HCl) solution, which is safe for plastics. Subsequently, PS networks are dissolved in toluene to form nonconductive Al complementary islands on the substrate (Figure 1e). Gold (Au) is deposited onto Al islands by thermal evaporation (Figure 1f). As Au is inert to chemicals/oxygen and has a suitable work function for hole injection in the latter OLED device application, it is used as the transparent

https://dx.doi.org/10.1021/acsami.0c07299
ACS Appl. Mater. Interfaces 2020, 12, 31687−31695

electrode material in our work. The Al isolated islands are lifted off in a 10% HCl solution to form interconnected Au TMM electrodes on the substrate (Figure 1g). In the first patterning process, the polymer is blade-coated to form interconnected polymer networks. After Al deposition and etching, polymer networks are lifted off, leaving isolated Al islands, the negative of the polymer network. Au is then deposited and Al is etched, leaving a Au interconnected network that duplicates the initial polymer networks. In Table S1, we compare this technique with other methods for flexible transparent electrodes including electron-spun polymer fiber networks, grain boundary lithography, and nanosphere lithography.[15,18−20,23,27,28]

2.2. Morphology Characterizations. Figure 2 shows the morphology of the film in each fabrication step. Large-area uniformities of microstructures are characterized by microscope images in Figure 2a−f, while the details can be observed from high-magnification scanning electron microscopy (SEM) images in Figure 2a′−f′. From Figure 2a′, it can be clearly seen that spheres gather together but are separated from each other after blade-coating, without forming interconnected networks. The PS spheres could slightly deform, melt together, and form fully interconnected polymer networks in the annealing process, which is shown in Figure 2b,b′. In comparison, the centrifugal force in the spin-coating process interrupts the formation of self-assembled patterns and generates inhomogeneous polymer micromesh networks (Figure S1). Both the Al and Au layers are produced using a standard thin-film deposition process that yields high-quality films, shown in Figure 2c,c′,e,e′. Figure 2d,d′ shows the morphology of Al islands left on the substrate after dissolving PS in toluene. Depositing the Au layer onto Al islands results in a color change in the microscopy image (Figure 3e) and decreased contrast in the SEM image (Figure 3e′). After dissolving the Al islands in a dilute HCl solution, we get the remaining film, which consists of uniform metal micromesh networks duplicated from polymer networks, which is flexible and transparent (Figures 2f,f′).

Nanosphere lithography patterns the metal by making use of the gap between close-packed nanospheres.[15] The close-packed nanosphere monolayer arrangement is crucial for the high optoelectrical performance of transparent electrodes in nanosphere lithography, but has strict requirements in terms of substrate energy and flatness and is also very challenging for large-area fabrication. Our process does not require a polymer sphere monolayer arrangement and provides a method to create transparent conductors on flexible substrates, which is compatible with large-area fabrication. The PS spheres are not arranged in a single layer in the blade-coating process, which results in the uneven heights of the PS film (the black line in Figure S2), but this does not reduce the optoelectronic performance of the electrodes. The collapse of the polymer spheres in the annealing process decreased the thickness of polymer networks (from around 300 nm to around 600 nm) (the red line in Figure S2). In this work, 6 nm Cr for the adhesive layer and a 34 nm Au film were used to guarantee the conductivity and transmittance of the metal networks. To make sure that the etching solution can spread to PS networks and Al islands in the two lift-off processes, the thickness of the Al film (120 nm used in this work) should lie between the thickness of polymer networks and the Au film. From the SEM image in Figure 2f′, it can be seen that the Au film does not have raised parts at the edges, which is attributed to the thin-film deposition process yielding high-quality films and a wet-etching chemical process without an external mechanical force.

2.3. Tunable Performances of TMM Electrodes. We aim to fabricate high-performance TMM electrodes, which can be used in thin-film organic electronics, such as organic light-emitting diodes. Generally, the organic layer is very thin for the thin-film optoelectronic devices, which hinders the application of many TMM electrodes with high conductivity and transparency but with large roughness. Therefore, low roughness is a critical factor for the conductors in thin-film devices.[29] Due to the flexibility and non-negligible static electricity effect of the plastic, it is always challenging to perform the large-area surface morphology measurements without deviation for the thin-film layer on plastics by atomic force microscopy (AFM). In the experiment, we evaporated the metal film on glass and calibrated the deposited metal thickness , which is shown in Figure S3. The results from height measurements on the PET substrate and glass are compared to demonstrate the variations in Figure S4. It is shown that the height of mesh structures on the PET substrate has an acceptable variation below 5 nm with that on the glass. Figure 3a shows the 3D AFM surface morphology for an area of 30 μm × 30 μm of the metal networks on the PET substrate, which consists of 6 nm Cr and 34 nm Au. The surface of the networks displays a low root-mean-square roughness (Rq) of about 20.0 nm, which is much smaller than that of many other reported metal networks.[18,30]Figure 3b shows the false-color SEM image of TMM electrodes up to 2 mm, which confirms the uniformity of micromesh structures. The structures and performance of the TMM electrodes can be tuned by adjusting the PS particle suspension concentration from 35 to 65 mg/mL. At a lower solution concentration, the micromesh network has narrower widths and bigger spaces, which can be seen from the SEM images of the metal meshes created from the tunable PS particle suspension solutions of concentrations 65, 50, and 40 mg/mL in Figures 3b−d. By decreasing the suspension concentration, the electrode's optical transmittance gradually increases (shown by blue dots in Figure 3e), whereas its electrical conductivity decreases (shown by black dots in Figure 3e). At the solution concentration of 35 mg/mL, the disconnection of micromesh network branches results in a significant decrease in the conductivity, as highlighted by the red circle in Figure S5a. More locations are disconnected at lower concentrations (Figure S5b) and this induces nonconductivity of the networks. The electrodes can achieve an optical transmittance of 86%, with the electrical conductance around 80 Ω sq^{-1} at a solution concentration of 35 mg/mL (marked as condition 1). At a higher concentration of 40 mg/mL (marked as condition 2), the TMM electrodes have a better conductivity of 19.7 Ω $sq^{-1}$with an optical transmittance of 80%. We also investigated the optoelectronic performance of the mesh electrodes with regard to varied Au film thicknesses. Figure S6 shows the transmittance and sheet resistance for a continuous metal film consisting of 6 nm of Cr and varied thicknesses of Au. Au films with thicknesses of 9, 17, 26, and 34 nm were investigated. The thinner film exhibits slightly better transmittance with a sacrificial loss in the conductivity. However, the bare-metal film with 6 nm Cr and 9 nm Au displays a resistance of 766 kΩ sq^{-1}, which is very high and does not meet the requirement for conductive electrodes. We have also studied and compared the transmittance and resistance for mesh electrodes with Au thicknesses of 17, 26, and 34 nm. As shown in Figure S7, at the same blade-coating solution concentration, increasing the metal thickness reduces the sheet resistance without significantly

https://dx.doi.org/10.1021/acsami.0c07299
ACS Appl. Mater. Interfaces 2020, 12, 31687−31695

changing the transmittance of the film. The reason is that the transmittance of the mesh electrodes is mainly determined by the apertures in the film, formed by the etched Al islands.

Figure 3f shows the relationship between the transmittance of the mesh at 550 nm (T_{550}) as a function of sheet resistance (R_{sheet}). The quality of a transparent conductor can be described by its figure of merit (FoM), which is conventionally a reliable indicator derived from its fundamental electrical and optical constants. An expression to determine the FoM of a conductor based on the relationship between direct current conductivity (σ_{dc}) and optical conductivity is shown in the following equation[3,37]

$$\sigma_{dc}/\sigma_{opt} = 188.5/(R_{sheet}\cdot(T_{550nm}^{-1/2}-1))$$

Higher ratios of σ_{dc}/σ_{opt} can be translated to higher FoM values or better $T - R_{sheet}$ trade-off, which indicates higher transmittance for a given R_{sheet} or a lower R_{sheet} for a given transmittance. Therefore, a high FoM is desired to achieve excellent device performance. FoM with a value of 35 is the minimum requirement for industrial/commercial viability. In this work, FoM for the mesh electrodes fabricated under condition 2 is around 81. Another FoM can be defined as $\phi_{TC} = T_{550nm}^{10}/R_{sheet}$ (Ω^{-1}).[38] The ϕ_{TC} of our mesh electrodes under the optimized condition 1 (2.7×10^{-3} Ω^{-1}) and condition 2 (5.5×10^{-3} Ω^{-1}) can be plotted as a function of $T_{550\ nm}$, as depicted in Figure 3e. For the purpose of comparison, the optoelectronic performances of other transparent electrodes (e.g., carbon nanotubes (CNT),[5] graphene,[31,32] PEDOT:PSS,[33] Ag nanowires (Ag NWs),[5] Ag grid combined with Ag NWs,[34] and metal meshes[3,17−21,23,35,36]) extracted from the literature are also presented in Figures 3f,g. Our TMM electrode's optoelectronic performances are comparable to the ones based on CNTs, graphene, Ag NWs, and metal meshes fabricated by other techniques. The resistance of the Au TMM electrode is slightly higher than those of the metal meshes in some studies, which results from the incompletely connected metal branches duplicated from the spontaneously self-assembled polymer networks. The transmittance of the TMM electrode in this work is of the same order of magnitude as those obtained in other approaches developed for transparent electrodes (between 80 and 90%). It is notable that the comparison of performance given in Figure 3f does not take into account all of the important performance properties required for an industrial flexible transparent electrode application: ability of the transparent electrode adapted to flexible films, ability for large-area fabrication, low-temperature process, and high efficiency of the deposition process. The uniformity and reproducibility of the TMM electrodes are limited by the blade-coating setup in the laboratory, which has one problem: the deposited film demonstrates nonuniform thickness along the blade-coating direction. In our lab, the TMM size is limited by the blade size with 6 cm width. A plastic substrate (10 cm × 10 cm) is used for blade-coating and the uniform printing range is around 6 cm, which is the region 3−9 cm away from the reservoir. Therefore, the maximum uniform and repeatable size of the TMM film is 6 cm × 6 cm in this study. However, the uniformity of the blade-coated film can be improved by a modified blade-coating system,[39,40] which thus endows our process with the possibility of being scalable and used for creating films on an industrial scale.

2.4. Transmittance and Flexibility of TMM Electrodes. TMM electrodes show flat transmittance spectra from 300 to 900 nm (Figure 4a). TMM electrodes prepared from a 40 mg/mL PS suspension can achieve over 85% transmittance, and the spectrum is shown as the red line in Figure 4a. In the following device application, the micromesh electrodes with 80% transmittance at 550 nm and 19.7 Ω sq^{-1} are used, and their transmittance spectrum is shown as the black line in Figure 4a. The mesh electrode is connected with an LED light bulb in series and provided a suitable power voltage (2.6 V), shown in Figure 4b. The LED light bulb can be lit at the provided voltage and the letters "Cal" on the paper can be clearly seen through the electrodes, demonstrating that TMM electrodes can be used as transparent conductors with mechanical flexibility. Our micromesh electrodes are also highly bendable. To test the mechanical flexibility of the micromesh structures, we fabricated metal electrodes on PET substrates and either bent the film to a radius of 1 mm (Figure 4c) or repetitively bent the film to 15 mm 3000 times (Figure 4d). No degradation in electrical conductivity in the electrodes is observed. In contrast, severe degradation in the conductivity of commercial ITO films is found after bending the film to a radius smaller than 10 mm, or bending the film to 15 mm more than 2 times.

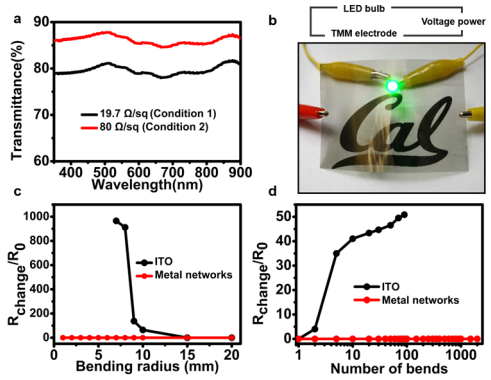

Figure 4. (a) Transmittance spectra of the Au TMM electrodes, showing flat transmittance in the broad range. (b) Picture of the transparent conductor using Au TMM electrodes. Schematic for the circuit shows that the Au TMM electrode is connected with an LED bulb in series and provided a voltage power of 2.6 V. (c, d) Mechanical test of the Au TMM electrodes. Resistance change for the Au TMM electrodes and ITO electrodes on a PET substrate for a series of bending radii (c), and after cycles at a bending radius of 15 mm (d).

2.5. Printing OLEDs Using TMM Electrodes. We printed OLEDs using metal mesh electrodes as transparent anodes. The structure of the printed OLEDs using TMM electrodes is shown in Figure 5a. In the device, the material layers consist of the Au TMM anode, PEDOT:PSS as the hole-transporting layer, an electron-blocking layer, an active layer, and a Ca/Al cathode. Here, the active layer is from a blend of poly((9,9-dioctylfluorene-2,7-diyl)-*alt*-(2,1,3-benzothiadiazole-4,8-diyl)) (F8BT) and poly(9,9-dioctylfluorene-*co*-*n*-(4-butylphenyl)-diphenylamine) (TFB).[26] TFB also works as an electron-blocking layer. For electrode materials, it is crucial to get a matched work function for electron/hole injection for a high yield of OLED devices. Au has a suitable work function for hole injection, which is shown from the energy-level diagram of the stack in Figure 5b. Organic layers including PEDOT:PSS, TFB, and F8BT:TFB were all blade-coated (Figure 5c) on the Au mesh electrodes under optimized conditions to get desired thickness PEDOT:PSS (70 nm), TFB (5−10 nm), and TFB:F8BT (100 nm). AFM is used to characterize the blade-coated layer

https://dx.doi.org/10.1021/acsami.0c07299
ACS Appl. Mater. Interfaces 2020, 12, 31687−31695

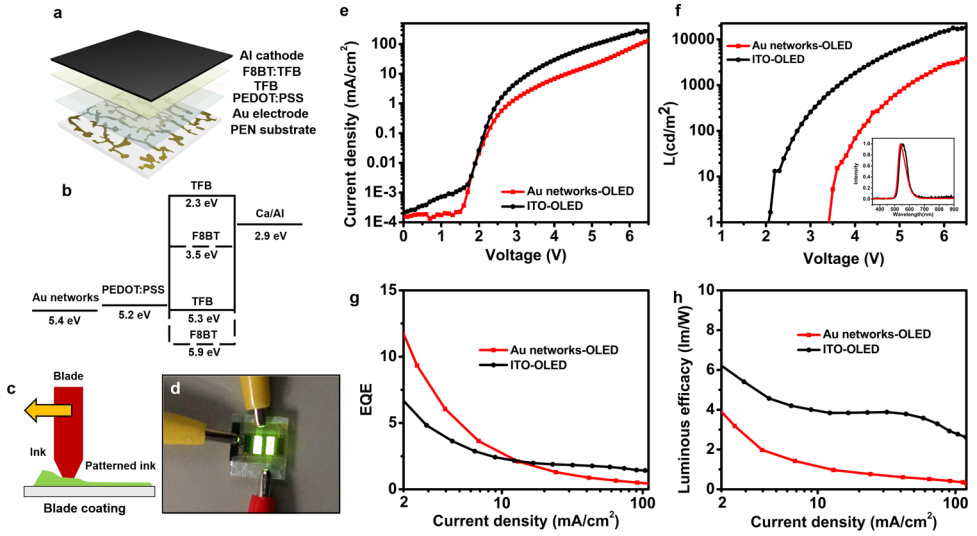

Figure 5. Printed OLEDs using the Au TMM electrodes. (a) Structure of the OLEDs. (b) Corresponding energy-level diagram of each layer. (c) Schematic for blade-coating semiconductors on the substrate. (d) Pictures of two OLED pixels operated at 5 V simultaneously. The emission area for each OLED device is 0.074 cm^2. (e–h) Device characterization for the OLEDs structured on a Au mesh electrode (red line) and an ITO substrate (black line). Plots of current-density versus voltage (J–V) (e), luminance versus voltage (L–V) (f), external quantum efficiency versus current density (EQE–J) (g), and luminous efficacy versus current density (h). Inset in (f): normalized emission spectrum of the OLEDs fabricated on Au networks and an ITO substrate.

(PEDOT:PSS, TFB, F8BT:TFB) on the Au mesh in the OLED device to show the height change in the whole process. After each layer coating, the height does not show distinct differences from the Au structure and the PEN substrate, displayed in Figure S8. The reason is that compared to the blade height (50 or 200 μm) for organic materials in the experiment, the height difference (below 50 nm) of the Au mesh and the PEN substrate is negligible and thus has little effect on the thickness of organic films on the Au mesh or PEN substrate. To describe the device structure more clearly, the cross-section schematic for the device is displayed in Figure S9. AFM was further used to characterize the sample with an area of 3 μm × 3 μm to evaluate the roughness for each device layer. As shown in Figure S10, the surface displays decreasing roughness after the coating of more layers (PEDOT:PSS, TFB, F8BT:TFB) on the Au mesh (Rq for the Au layer is 1.156 nm, Rq for the layer after PEDOT:PSS coating is 1.139 nm, Rq for the layer after TFB coating is 0.879 nm, and Rq for the layer after F8BT:TFB coating is 0.677 nm). The picture of a uniform green-emitting array is shown in Figure 5d. The current-density–voltage (J–V), luminance–voltage (L–V), external quantum efficiency (EQE)–J, and luminous efficacy–J characteristics of the OLEDs fabricated on Au mesh networks/PEN and ITO/PEN are presented in Figure 5e–h. The device fabricated on the Au electrode shows a similar green emission spectrum to that on ITO (inset in Figure 5f), without a shift of the emission peak. The as-fabricated OLED device shows a clear diode behavior without abnormal discontinuities and is turned on at 3.4 V. The OLED device can achieve a luminance of over 4000 cd/m^2 at 6.5 V. At a luminance of 100 cd/m^2, the printed OLED device shows a drive voltage of 4.1 V, a current density of 7.6 mA/cm^2, an EQE of 3.6%, and a luminous efficacy of 1.4 lm/W. Compared with the performance of the ITO-based device summarized in Table S2, our device shows weaker luminance, lower EQE, and higher turn-on voltage. The decrease in the device performance structured on Au mesh electrodes is caused by exposure to ambient air before encapsulation (more experimental details are shown in Figure S11), chemical contamination in the etching process, slightly bigger surface roughness, and lower transmittance than ITO in the Au mesh electrodes.[41−44] Further patterning, deep cleaning, or/and surface modification of the mesh electrodes are believed to enhance the performance of Au-mesh-based OLEDs. Nevertheless, the OLED device using metal micromesh electrodes shows uniform emission and stable performance throughout the characterization. We compare the performance and fabrication technique between our device and others based on nanowire, graphene, or metal electrodes, as shown in Table S3.[13,17,37,45,46] The device on prepared mesh electrodes shows a comparatively lower turn-on voltage and a higher maximum luminescent intensity among these devices. The printed OLEDs based on Au micromesh electrodes demonstrate good potential for fabricating flexible, large-area, and high-performance electronics and sensors.

One of the most critical bottlenecks that limit the mechanical durability of flexible optoelectronic devices is the brittleness of ITO. In this work, we have succeeded in improving the flexibility of transparent electrodes by replacing ITO with Au mesh electrodes. However, the organic devices including OLEDs have multilayered structures (semiconductor layers, electrodes, and encapsulation layer), and the flexibility of the devices is determined not only by the brittleness of transparent electrodes but also by the durability of other layers as well as interfacial properties such as adhesion between each layer. This is an important research direction for further improvement of the mechanical robustness of the flexible optoelectronic devices. The unique porous structure enables large stretchability of Au mesh electrodes, which are promising for applications in foldable optical electronics and musclelike transducers.[20] Investigating how to fabricate or transfer mesh structures on/to stretchable substrates is another attractive research area for further application of transparent electrodes in stretchable electronics.

https://dx.doi.org/10.1021/acsami.0c07299
ACS Appl. Mater. Interfaces 2020, 12, 31687−31695

3. CONCLUSIONS

In conclusion, we developed a print-compatible process to create a thin film of Au TMM electrode with a thickness below 50 nm. The Au TMM electrodes are inert to air and radiation energy, flexible, and mechanically durable. The conductivity and transmittance of TMM electrodes could be tuned by the space length and mesh width at gradually increasing blade-coating solution concentration, and a conductivity of 19.7 Ω sq^{-1} at 80% transmittance was achieved. The electrodes also exhibited superior flexibility, with no degradation in conductivity at the smallest bending radius of 1 mm or repeated bending over 3000 times at a radius smaller than 15 mm. To demonstrate its feasibility in high-performance thin-film optoelectronics, printing OLEDs using Au TMM electrodes with low turn-on voltage and bright luminance were successfully fabricated, which is one of the most efficient OLEDs ever reported using metal mesh electrodes. This fabrication technique provides a low-cost and high-throughput transparent electrode method for printed electronics over large areas.

4. EXPERIMENTAL METHODS

4.1. Blade-Coater Setup. A doctor blade with 6 cm width (Zehntner ZUA 2000.60) was used to coat a PS bead suspension in water (600 nm diameter, Sigma-Aldrich), PEDOT:PSS (Clevios AI4083, Heraeus), TFB, and F8BT:TFB. Linear actuators (Servo City) were set up inside and outside a glovebox, the heights of which were adjusted so as to carry out the coating process on the substrate placed on a hot plate.

4.2. TMM Electrode Fabrication. PET (Dupont Teijin Films, Melinex ST504) or planarized PEN (Dupont Teijin Films, Optfine PQA1) was used as received. The substrate was plasma-treated for 60 s at 50 W power before blade-coating. PS (120 μL) suspension was blade-coated with a blade height of 300 μm at 1 cm^{-1} on a hot plate set to 85 °C. The temperature of the hot plate was increased to 120 °C right after blade-coating and the substrate was annealed at that temperature for 15 min. The sample was transferred into a thermal evaporator for deposition of 120 nm Al (99.999%, Aci Alloys Inc). The sample was cleaned in toluene under sonication for 30 min, then rinsed by acetone and isopropanol, and blow-dried by compressed air. The sample was transferred into a thermal evaporator for deposition of 6 nm Cr and Au with varied thicknesses (99.99%, Kurt J. Lesker). The sample was then placed face down and allowed to float over a 10% HCl solution overnight; then, it was ultrasonically cleaned in deionized water, isopropanol, and acetone for 2 min separately. The sample was blow-dried by compressed air.

4.3. Printed OLED Fabrication. The Au mesh/PEN substrate was ultrasonically rinsed in ethanol for 15 min and blow-dried before the device fabrication. The 27 mm × 60 mm substrate was then laminated on a 10 cm × 10 cm glass carrier using an adhesive gel film (GEL-PaK) to give rigidity during processing. The Au mesh/PEN or patterned ITO/PEN substrate (used as received from Cambridge Display Technology Limited) was baked in a vacuum hot plate at 80 °C overnight and then taken out in ambient air and heated on a hot plate at 180 °C for 30 min. The substrate was treated with plasma for 10 s and the entire surface was treated with (heptadecafluoro-1,1,2,2-tetrahydrodecyl)trichlorosilane (Gelest SIH5841.0) for 20 min under light vacuum (0.1−1 Torr). The blade-coated area (17 mm × 60 mm) was exposed by masking the substrate with Kapton tape before it was plasma treated for 90 s. PEDOT:PSS (28 μL) was blade-coated with a blade height of 50 μm at 1 cm s^{-1} on a hot plate set to 90 °C. The temperature of the hot plate was increased to 130 °C right after blade-coating and the sample was annealed for 10 min. The sample was then placed inside the glovebox and TFB (6 mg/mL in *o*-xylene) was blade-coated with 23 μL of solution and a blade height of 50 μm at 1 cm s^{-1} on the hot plate set to 65 °C, and then, the sample was annealed at 180 °C for 60 min. After annealing, the hot plate was set back to 65 °C again and the emission layer, a blend of F8BT mixed with TFB with a weight ratio of 9:1 (15 mg/mL in *o*-xylene), was blade-coated with 28 μL of solution and a blade height of 200 μm at 1 cm s^{-1}. The sample was annealed at 140 °C for 30 min and then transferred into a thermal evaporator for deposition of calcium (99.5%, STREM CHEMICALS) and aluminum. The device emission area is defined by the overlap area of the anode, the active layer, and the cathode. The area of the OLED emission layer in this work is 0.074 cm^2.

4.4. Device Encapsulation. The process varies for the devices structured on a Au mesh/PEN sample and an ITO/PEN sample, which is shown in Figure S11. After evaporation, the Au mesh/PEN sample was taken out from the glovebox and bonded with wires for measurement. Then, the Au mesh/PEN sample was transferred back into the glovebox. A drop of UV curable epoxy was placed on top of an active pixel. For the patterned ITO/PEN substrate, a drop of UV curable epoxy was placed on top of an active pixel and pressed gently with a precut plastic film after evaporation. Both samples were placed under UV radiation with a UV lamp (BHK INC.) for 30 min to cure the epoxy.

4.5. Device Characterization. The fabricated devices were measured using a Keithley 2601 and a Keithley 2400 to study the *J*−*V* characteristics and to take photodiode readings, respectively. Emission spectra and total flux were measured using a Keithley 2601 and a spectrometer (SP-75, Orboptronix) equipped with an integrating sphere.

4.6. Surface Profile Measurement. The sample was firmly mounted on a glass/gel−film system. A Dektak profiler (Veeco 6M) was used to measure the film thickness.

4.7. Atomic Force Microscopy (AFM) Measurements. The sample was cut into small pieces (about 1 cm × 1 cm) and sucked at the AFM stage. Measurements were done on a Park system AFM.

4.8. Transmittance Measurements. UV-2600 was used to measure the UV−vis transmittance spectra.

4.9. SEM Measurements. The sample was precoated with a thin film of Au/Pd for better conductivity before doing SEM measurements. Images were taken on a Zeiss Gemini SEM.

■ ASSOCIATED CONTENT

Supporting Information

The Supporting Information is available free of charge at https://pubs.acs.org/doi/10.1021/acsami.0c07299.

Comparison of flexible transparent electrodes in the literatures and our work (Table S1); inhomogenous microstructures of polymer sphere networks formed by spin-coating (Figure S1); surface profile measurement on polymer sphere networks before and after annealing (Figure S2); metal films were patterned with Kapton tape and evaporated on the glass to characterize the film thickness of Cr and Au in the experiment (Figure S3); height results of the mesh structures on the PET substrate (Figure S4); disconnected polymer sphere networks forming under low solution concentration (Figure S5); transmittance and sheet resistance of the continuous metal film with different Au thickness (Figure S6); transmittance and sheet resistance of the mesh electrodes with respect to blade-coating solution concentration and Au film with the varied thickness are displayed in graphs (Figure S7); AFM height images and profiles for each layer of OLED device on the PEN substrate (Figure S8); cross-section schematic for OLED structures (Figure S9); AFM images for 3 μm × 3 μm scan area to show the surface roughness of each layer in the device (Figure S10); schematic for the OLED device encapsulation structured on ITO/PEN (Figure S11); summary of device drive voltage, current density, luminous efficiency and EQE at luminance 100 cd/m^2 (Table S2); comparison of OLED deviceperformance based on graphene composite, Ag

https://dx.doi.org/10.1021/acsami.0c07299
ACS Appl. Mater. Interfaces 2020, 12, 31687−31695

nanowire, Cu mesh and our metal mesh (Table S3); references (PDF)

AUTHOR INFORMATION

Corresponding Author

Ana C. Arias − *Department of Electrical Engineering and Computer Sciences, University of California Berkeley, Berkeley, California 94720, United States;* orcid.org/0000-0001-6866-5250; Email: acarias@eecs.berkeley.edu

Authors

Juan Zhu − *Department of Electrical Engineering and Computer Sciences, University of California Berkeley, Berkeley, California 94720, United States; Institute of Physics & University of Chinese Academy of Sciences, Chinese Academy of Sciences, Beijing 100190, P. R. China;* orcid.org/0000-0003-3341-2215

Donggeon Han − *Department of Electrical Engineering and Computer Sciences, University of California Berkeley, Berkeley, California 94720, United States*

Xiaodong Wu − *Department of Electrical Engineering and Computer Sciences, University of California Berkeley, Berkeley, California 94720, United States*

Jonathan Ting − *Department of Electrical Engineering and Computer Sciences, University of California Berkeley, Berkeley, California 94720, United States*

Shixuan Du − *Institute of Physics & University of Chinese Academy of Sciences, Chinese Academy of Sciences, Beijing 100190, P. R. China;* orcid.org/0000-0001-9323-1307

Complete contact information is available at: https://pubs.acs.org/10.1021/acsami.0c07299

Notes

The authors declare no competing financial interest.

ACKNOWLEDGMENTS

This work was supported in part by the National Science Foundation (NSF) under the ECCS Grant No. 1610899, the International Partnership Program of Chinese Academy of Sciences (No. 112111KYSB20160061), and the National Natural Science Foundation of China (No. 61888102). The OLED materials were donated by Cambridge Display Technology Limited. This material is based, in part, on research sponsored by the Air Force Research Laboratory under agreement number FA8650-15-2-5401, as conducted through the flexible hybrid electronics manufacturing innovation institute, NextFlex. The U.S. Government is authorized to reproduce and distribute reprints for governmental purposes notwithstanding any copyright notation thereon. The views and conclusions contained herein are those of the authors and should not be interpreted as necessarily representing the official policies or endorsements, either expressed or implied, of the Air Force Research Laboratory or the U.S. Government. Thanks are due to Professor James W Evans, Carol Baumbauer, and Jasmine Jan for helpful discussions.

REFERENCES

(1) Hecht, D. S.; Hu, L.; Irvin, G. Emerging Transparent Electrodes Based on Thin Films of Carbon Nanotubes, Graphene, and Metallic Nanostructures. *Adv. Mater.* **2011**, *23*, 1482−1513.

(2) Ellmer, K. Past Achievements and Future Challenges in the Development of Optically Transparent Electrodes. *Nat. Photonics* **2012**, *6*, 809−817.

(3) Lee, H. B.; Jin, W. Y.; Ovhal, M. M.; Kumar, N.; Kang, J. W. Flexible Transparent Conducting Electrodes Based on Metal Meshes for Organic Optoelectronic Device Applications: A Review. *J. Mater. Chem. C* **2019**, *7*, 1087−1110.

(4) Ye, S.; Rathmell, A. R.; Chen, Z.; Stewart, I. E.; Wiley, B. J. Metal Nanowire Networks: The Next Generation of Transparent Conductors. *Adv. Mater.* **2014**, *26*, 6670−6687.

(5) Guo, C. F.; Ren, Z. Flexible Transparent Conductors Based on Metal Nanowire Networks. *Mater. Today* **2015**, *18*, 143−154.

(6) Kim, E.; Cho, H.; Kim, K.; Koh, T. W.; Chung, J.; Lee, J.; Park, Y.; Yoo, S. A Facile Route to Efficient, Low-Cost Flexible Organic Light-Emitting Diodes: Utilizing the High Refractive Index and Built-in Scattering Properties of Industrial-Grade Pen Substrates. *Adv. Mater.* **2015**, *27*, 1624−1631.

(7) Wang, B.; Facchetti, A. Mechanically Flexible Conductors for Stretchable and Wearable E-Skin and E-Textile Devices. *Adv. Mater.* **2019**, *31*, No. e1901408.

(8) Tong, J.; Xiong, S.; Zhou, Y.; Mao, L.; Min, X.; Li, Z.; Jiang, F.; Meng, W.; Qin, F.; Liu, T.; Ge, R.; Fuentes-Hernandez, C.; Kippelen, B.; Zhou, Y. Flexible All-Solution-Processed All-Plastic Multijunction Solar Cells for Powering Electronic Devices. *Mater. Horiz.* **2016**, *3*, 452−459.

(9) Zhu, J.; Li, J.; Zhong, Q.; Wang, H.; Huang, L.; Fontein, F.; Hu, L.; Liu, R.; Fuchs, H.; Wang, W.; Wang, Y.; Chi, L. Lithography Compatible, Flexible Micro-Organic Light-Emitting Diodes by Template-Directed Growth. *Small Methods* **2019**, *3*, No. 1800508.

(10) Ostfeld, A. E.; Catheline, A.; Ligsay, K.; Kim, K.-C.; Chen, Z.; Facchetti, A.; Fogden, S.; Arias, A. C. Single-Walled Carbon Nanotube Transparent Conductive Films Fabricated by Reductive Dissolution and Spray Coating for Organic Photovoltaics. *Appl. Phys. Lett.* **2014**, *105*, No. 253301.

(11) Ok, K. H.; Kim, J.; Park, S. R.; Kim, Y.; Lee, C. J.; Hong, S. J.; Kwak, M. G.; Kim, N.; Han, C. J.; Kim, J. W. Ultra-Thin and Smooth Transparent Electrode for Flexible and Leakage-Free Organic Light-Emitting Diodes. *Sci. Rep.* **2015**, *5*, No. 9464.

(12) Zeng, X. Y.; Zhang, Q. K.; Yu, R. M.; Lu, C. Z. A New Transparent Conductor: Silver Nanowire Film Buried at the Surface of a Transparent Polymer. *Adv. Mater.* **2010**, *22*, 4484−4488.

(13) Lee, J.; Lee, P.; Lee, H.; Lee, D.; Lee, S. S.; Ko, S. H. Very Long Ag Nanowire Synthesis and Its Application in a Highly Transparent, Conductive and Flexible Metal Electrode Touch Panel. *Nanoscale* **2012**, *4*, 6408−6414.

(14) Kim, A.; Won, Y.; Woo, K.; Kim, C.-H.; Moon, J. Highly Transparent Low Resistance Zno/Ag Nanowire/Zno Composite Electrode for Thin Film Solar Cells. *ACS Nano* **2013**, *7*, 1081−1091.

(15) Zhang, J.; Li, Y.; Zhang, X.; Yang, B. Colloidal Self-Assembly Meets Nanofabrication: From Two-Dimensional Colloidal Crystals to Nanostructure Arrays. *Adv. Mater.* **2010**, *22*, 4249−4269.

(16) Wang, Y.; Zhang, M.; Lai, Y.; Chi, L. Advanced Colloidal Lithography: From Patterning to Applications. *Nano Today* **2018**, *22*, 36−61.

(17) Kang, M. G.; Guo, L. J. Nanoimprinted Semitransparent Metal Electrodes and Their Application in Organic Light-Emitting Diodes. *Adv. Mater.* **2007**, *19*, 1391−1396.

(18) Wu, H.; Kong, D.; Ruan, Z.; Hsu, P. C.; Wang, S.; Yu, Z.; Carney, T. J.; Hu, L.; Fan, S.; Cui, Y. A Transparent Electrode Based on a Metal Nanotrough Nwtwork. *Nat. Nanotechnol.* **2013**, *8*, 421−425.

(19) Yang, J.; Bao, C.; Zhu, K.; Yu, T.; Xu, Q. High-Performance Transparent Conducting Metal Network Electrodes for Perovksite Photodetectors. *ACS Appl. Mater. Interfaces* **2018**, *10*, 1996−2003.

(20) Guo, C. F.; Sun, T.; Liu, Q.; Suo, Z.; Ren, Z. Highly Stretchable and Transparent Nanomesh Electrodes Made by Grain Boundary Lithography. *Nat. Commun.* **2014**, *5*, No. 3121.

(21) Chauvin, A.; Txia Cha Heu, W.; Buh, J.; Tessier, P.-Y.; El Mel, A.-A. Vapor Dealloying of Ultra-Thin Films: A Promising Concept for the Fabrication of Highly Flexible Transparent Conductive Metal Nanomesh Electrodes. *npj Flexible Electron.* **2019**, *3*, 1−6.

(22) Moon, C.-J.; Kim, I.; Joo, S.-J.; Chung, W.-H.; Lee, T.-M.; Kim, H.-S. Flash Light Sintering of Ag Mesh Films for Printed Transparent Conducting Electrode. *Thin Solid Films* **2017**, *629*, 60−68.
(23) Jiang, Z.; Fukuda, K.; Xu, X.; Park, S.; Inoue, D.; Jin, H.; Saito, M.; Osaka, I.; Takimiya, K.; Someya, T. Reverse-Offset Printed Ultrathin Ag Mesh for Robust Conformal Transparent Electrodes for High-Performance Organic Photovoltaics. *Adv. Mater.* **2018**, *30*, No. e1707526.
(24) Pierre, A.; Sadeghi, M.; Payne, M. M.; Facchetti, A.; Anthony, J. E.; Arias, A. C. All-Printed Flexible Organic Transistors Enabled by Surface Tension-Guided Blade Coating. *Adv. Mater.* **2014**, *26*, 5722.
(25) Pierre, A.; Gaikwad, A.; Arias, A. C. Charge-Integrating Organic Heterojunction Phototransistors for Wide-Dynamic-Range Image Sensors. *Nat. Photonics* **2017**, *11*, 193−199.
(26) Han, D.; Khan, Y.; Ting, J.; King, S. M.; Yaacobi-Gross, N.; Humphries, M. J.; Newsome, C. J.; Arias, A. C. Flexible Blade-Coated Multicolor Polymer Light-Emitting Diodes for Optoelectronic Sensors. *Adv. Mater.* **2017**, *29*, No. 1606206.
(27) Hossain, M.; Kumar, G. S.; Barimar Prabhava, S. N.; Sheerin, E. D.; McCloskey, D.; Acharya, S.; Rao, K. D. M.; Boland, J. J. Transparent, Flexible Silicon Nanostructured Wire Networks with Seamless Junctions for High-Performance Photodetector Applications. *ACS Nano* **2018**, *12*, 4727−4735.
(28) Hong, S.; Yeo, J.; Kim, G.; Kim, D.; Lee, H.; Kwon, J.; Lee, H.; Lee, P.; Ko, S. H. Nonvacuum, Maskless Fabrication of a Flexible Metal Grid Transparent Conductor by Low-Temperature Selective Laser Sintering of Nanoparticle Ink. *ACS Nano* **2013**, *7*, 5024−5031.
(29) Jung, S.; Lee, S.; Song, M.; Kim, D.-G.; You, D. S.; Kim, J.-K.; Kim, C. S.; Kim, T.-M.; Kim, K.-H.; Kim, J.-J.; Kang, J.-W. Extremely Flexible Transparent Conducting Electrodes for Organic Devices. *Adv. Energy Mater.* **2014**, *4*, No. 1300474.
(30) Hu, L.; Kim, H. S.; Lee, J. Y.; Peumans, P.; Cui, Y. Scalable Coating and Properties of Transparent, Flexible, Silver Nanowire Electrodes. *ACS Nano* **2010**, *4*, 2955−2963.
(31) Kim, K. S.; Zhao, Y.; Jang, H.; Lee, S. Y.; Kim, J. M.; Kim, K. S.; Ahn, J. H.; Kim, P.; Choi, J. Y.; Hong, B. H. Large-Scale Pattern Growth of Graphene Films for Stretchable Transparent Electrodes. *Nature* **2009**, *457*, 706−710.
(32) Bae, S.; Kim, H.; Lee, Y.; Xu, X.; Park, J. S.; Zheng, Y.; Balakrishnan, J.; Lei, T.; Kim, H. R.; Song, Y. I.; Kim, Y. J.; Kim, K. S.; Ozyilmaz, B.; Ahn, J. H.; Hong, B. H.; Iijima, S. Roll-to-Roll Production of 30-Inch Graphene Films for Transparent Electrodes. *Nat. Nanotechnol.* **2010**, *5*, 574−578.
(33) Kim, Y. H.; Sachse, C.; Machala, M. L.; May, C.; Müller-Meskamp, L.; Leo, K. Highly Conductive Pedot:Pss Electrode with Optimized Solvent and Thermal Post-Treatment for Ito-Free Organic Solar Cells. *Adv. Funct. Mater.* **2011**, *21*, 1076−1081.
(34) Ye, T.; Jun, L.; Kun, L.; Hu, W.; Ping, C.; Ya-Hui, D.; Zheng, C.; Yun-Fei, L.; Hao-Ran, W.; Yu, D. Inkjet-Printed Ag Grid Combined with Ag Nanowires to Form a Transparent Hybrid Electrode for Organic Electronics. *Org. Electron.* **2017**, *41*, 179−185.
(35) Gao, T.; Wang, B.; Ding, B.; Lee, J. K.; Leu, P. W. Uniform and Ordered Copper Nanomeshes by Microsphere Lithography for Transparent Electrodes. *Nano Lett.* **2014**, *14*, 2105−2110.
(36) Bao, C.; Yang, J.; Gao, H.; Li, F.; Yao, Y.; Yang, B.; Fu, G.; Zhou, X.; Yu, T.; Qin, Y.; Liu, J.; Zou, Z. In Situ Fabrication of Highly Conductive Metal Nanowire Networks with High Transmittance from Deep-Ultraviolet to near-Infrared. *ACS Nano* **2015**, *9*, 2502−2509.
(37) Jin, W. Y.; Ginting, R. T.; Ko, K. J.; Kang, J. W. Ultra-Smooth, Fully Solution-Processed Large-Area Transparent Conducting Electrodes for Organic Devices. *Sci. Rep.* **2016**, *6*, No. 36475.
(38) Haacke, G. New Figure of Merit for Transparent Conductors. *J. Appl. Phys.* **1976**, *47*, 4086−4089.
(39) Youn, H.; Jeon, K.; Shin, S.; Yang, M. All-Solution Blade−Slit Coated Polymer Light-Emitting Diodes. *Org. Electron.* **2012**, *13*, 1470−1478.
(40) Chen, C.-Y.; Chang, H.-W.; Chang, Y.-F.; Chang, B.-J.; Lin, Y.-S.; Jian, P.-S.; Yeh, H.-C.; Chien, H.-T.; Chen, E.-C.; Chao, Y.-C. Continuous Blade Coating for Multi-Layer Large-Area Organic Light-Emitting Diode and Solar Cell. *J. Appl. Phys.* **2011**, *110*, No. 094501.
(41) Beierlein, T. A.; Brütting, W.; Riel, H.; Haskal, E. I.; Müller, P.; Rieß, W. Kelvin Probe Investigations of Metal Work Functions and Correlation to Device Performance of Organic Light-Emitting Devices. *Synth. Met.* **2000**, *111-112*, 295−297.
(42) Scott, J. C.; Malliaras, G. G.; Chen, W. D.; Breach, J. C.; Salem, J. R.; Brock, P. J.; Sachs, S. B.; Chidsey, C. E. D. Hole Limited Recombination in Polymer Light-Emitting Diodes. *Appl. Phys. Lett.* **1999**, *74*, 1510−1512.
(43) Wang, S.; Liu, Y.; Huang, X.; Yu, G.; Zhu, D. Phthalocyanine Monolayer-Modified Gold Substrates as Efficient Anodes for Organic Light-Emitting Diodes. *J. Phys. Chem. B* **2003**, *107*, 12639−12642.
(44) Zhu, J.; Fontein, F.; Wang, H.; Zhong, Q. G.; Li, C. L.; Li, J. P.; Wang, B.; Liao, L. S.; Wang, Y.; Huang, L. Z.; Fuchs, H.; Wang, W. C.; Chi, L. F. Micro Organic Light-Emitting Diodes Fabricated through Area-Selective Growth. *Mater. Chem. Front.* **2017**, *1*, 2606−2612.
(45) Chang, H.; Wang, G.; Yang, A.; Tao, X.; Liu, X.; Shen, Y.; Zheng, Z. A Transparent Flexible, Low-Temperature, and Solution-Processible Graphene Composite Electrode. *Adv. Funct. Mater.* **2010**, *20*, 2893−2902.
(46) Liang, J.; Li, L.; Tong, K.; Ren, Z.; Hu, W.; Niu, X. F.; Chen, Y. S.; Pei, Q. B. Silver Nanowire Percolation Network Soldered with Graphene Oxide at Room Temperature and Its Application for Fully Stretchable Polymer Light Emitting Diodes. *ACS Nano* **2014**, *8*, 1590−1600.

https://dx.doi.org/10.1021/acsami.0c07299
ACS Appl. Mater. Interfaces 2020, 12, 31687−31695